Negative quasiparticle shifts in phosphorene quantum dots

Jun Zhong, Jun Xie, and Weidong Sheng*
State Key Laboratory of Surface Physics and Department of Physics, Fudan University, Shanghai 200433, China

(Received 21 December 2020; revised 6 April 2021; accepted 24 May 2021; published 2 June 2021)

It is commonly believed that electron correlations would open up a quasiparticle gap in semiconductors. Contrary to this intuitive expectation, here we reveal that phosphorene quantum dots (PQDs) may exhibit just the opposite effect. By using a configuration interaction approach beyond the conventional double-excitation scheme, quasiparticle energies are calculated for hexagonal and rectangular PQDs in various dielectric environments. For the hexagonal PQD with a nominal gap of 2.26 eV, it is found that the quasiparticle shift decreases by more than 500 meV and eventually becomes negative when the effective dielectric constant is reduced from 20.0 to 5.0. For other trapezoidal, triangular, and rectangular PQDs, the quasiparticle shift exhibits a similar amount of decrement after the same change in the dielectric environment. Furthermore, the calculation by adopting the Rytova-Keldysh potential, which may be more suitable to describe two-dimensional screening, also shows a very similar result, although with smaller decrement of the quasiparticle shift. The origin of this anomalous quasiparticle shift is believed to be related to the long-range electron-electron interactions in the distinctive lattice structure of PQDs, as a similar phenomenon has never been found in graphene quantum dots.

DOI: 10.1103/PhysRevB.103.235405

I. INTRODUCTION

Generally speaking, the quasiparticle (QP) serves as the single most important concept to understand complicated phenomena in optical and transport processes in solids [1]. Narrowly speaking, QP energies are closely related to those required to add or remove one electron from the system and can be formulated within the many-body perturbation formalism [2]. The QP gap, also known as fundamental or transport gap, defined as the difference between ionization potential and electron affinity, is usually established by photoemission or inverse photoemission spectroscopy [3]. In the meantime, during the optical absorption process, the QP effect [4] combined with the excitonic effect [5] determines the optical gap of a many-electron system, although the total number of electrons in the system remains unchanged. In low-dimensional nanostructures such as graphene nanoflakes [6], electron correlations open up the QP gap, which is already enhanced by the quantum confinement effect [7]. Since the QP effect arises from the electron-electron interactions, it is commonly believed that a reduced screening effect would naturally increase the QP gap of the system.

For two-dimensional (2D) bulk semiconductors, a linear scaling relation has been shown between the QP gap Δ_{qp} and the exciton binding energy E_X [8], specifically, $\Delta_{qp} \approx 4E_X$ [9]. For 2D nanostructures, one needs to subtract the nominal single-particle gap Δ_{sp} from the QP gap Δ_{qp} to define the QP shift as

$$\Delta_{qs} = \Delta_{qp} - \Delta_{sp}, \tag{1}$$

in order to separate the QP effect from the quantum confinement effect appropriately. For graphene nanoflakes, the QP shift has been revealed to be almost identical to the exciton binding energy, i.e., $\Delta_{qs} \approx E_X$ [10], leaving the optical gap insensitive to the dielectric environments. In regard to excitons, it is fairly obvious that their binding energies increase when the screening effect is weakened. Back to QPs, it seems to be straightforward that the QP shift shall have the same behavior as the exciton binding energy. That is to say, the QP shift would always be positive. Specifically, if the screening effect can be described by an effective dielectric constant κ, $\Delta_{qs}(\kappa^{-1})$ would be an always positive and monotonically increasing function. This has been proven to be true for monolayer transition metal dichalcogenides WS_2 and WSe_2 [11] and graphene nanoflakes [12].

For phosphorene quantum dots, however, here we will show that $\Delta_{qs}(\kappa^{-1})$ is *not* an always monotonically increasing function and can even becomes *negative* as κ decreases. Since its first successful fabrication [13], layered black phosphorus (BP) or phosphorene nanostructures have a shown fascinating optical properties which promise potential applications in optoelectronics [14,15]. Moreover, phosphorene quantum dots (PQDs) are reported to be successfully prepared from the bulk BP crystal using liquid exfoliation methods [16]. The nanostructures fabricated by such a facile top-down approach in solution or glass can be as small as 5 nm in lateral size and 2–4 layers in thickness [17–19]. It is predicted that PQDs may reach an energy conversion efficiency of as high as 20% in solar energy conversion [20] and are thus very suitable to be an alternative candidate for highly efficient solar cells [21] as well as for ultrafast fiber lasers [22].

The studies of electronic structure have been reported for monolayer [23] and bilayer [24,25] PQDs. In the meantime, the optical response of phosphorene and PQDs have been

*shengw@fudan.edu.cn

 ©2021 American Physical Society

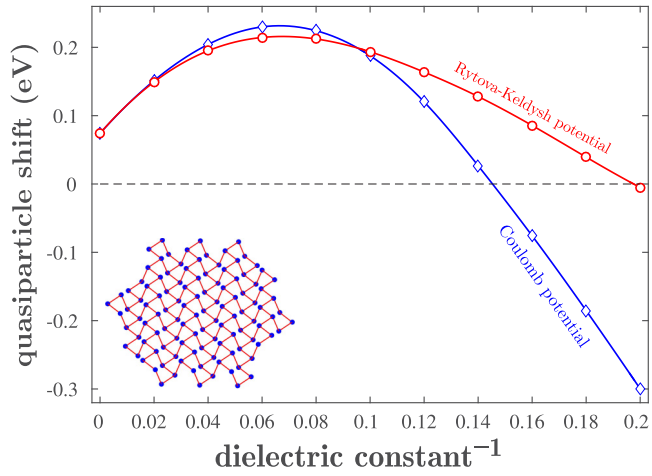

FIG. 1. Quasiparticle shifts calculated as a function of the inverse of the effective dielectric constant by using the Rytova-Keldysh potential (circular dots) or the conventional Coulomb interaction potential (diamond dots) for a hexagonal phosphorene quantum dot as depicted in the inset. The nominal gap of the PQD is 2.26 eV.

investigated by using the first-principles approach [26] as well as the empirical tight-binding method [27,28]. It has been recently reported that optical gaps in PQDs could be greatly suppressed by the strong screening effect [29]. There are two major factors playing an important role in determining the optical gap, namely, QP and excitonic effects. Since the latter has a quite transparent dependence on the dielectric environment, suppression of the optical gap can only be induced by the collapse of the QP gap.

II. MODEL AND METHOD

A schematic view of the first model system, a hexagonal phosphorene quantum dot, is shown in the inset of Fig. 1. The total number of phosphorus atoms is $N = 104$. The single-particle states in the monolayer PQD are calculated by using a tight-binding (TB) model with the parametrization obtained from *ab initio* calculations within the GW approximation as follows [30]:

$$\hat{H}_e = \sum_{i=1}^{N}\sum_{\sigma} E_{i\sigma} c_{i\sigma}^{\dagger} c_{i\sigma} + \sum_{i,j}^{N}\sum_{\sigma} (t_{ij} c_{i\sigma}^{\dagger} c_{j\sigma} + \text{H.c.}), \quad (2)$$

where $E_{i\sigma}$ is the energy of the electron at site i with spin σ, and t_{ij} is the hopping parameter between the ith and jth sites. It is noted that this is an effective one-band TB model, i.e., only one electron per phosphorus atom is included and therefore the total number of electrons, N_e, is equal to N for a charge neutral system. Due to the lattice symmetry, the on-site energies $E_{i\sigma}$ are equivalent for all lattice sites and are thus set to zero. There are a total of five intralayer hopping parameters, and the most important ones are those among the in-plane and out-of-plane nearest neighbors. The dangling bonds are passivated by ten hydrogen atoms to prevent the edge states from appearing in the middle of the energy spectrum [31].

It is noted that this TB parametrization reproduces both electron and hole states within the region of about 0.3 eV from the Γ point, which is considered to be well suited for the study of excitonic states in optical transitions [32]. The spin-orbit interaction is neglected in the tight-binding Hamiltonian because the coupling only induces a very small correction to the energy levels. Moreover, a recent experimental work reports layer-dependent exciton binding energies in few-layer black phosphorus and determines that a freestanding BP monolayer yields a large exciton binding energy of about 0.8 eV [33]. For comparison, we have studied the excitonic states by using the same TB model [29] and predict that the exciton binding energy shall reach 0.9–1.0 eV for a triangular PQD with minimum dielectric screening effect.

The single-particle states are obtained as $\psi_k = \sum_{i=1}^{N} a_k^i |i\rangle$ by solving the TB Hamiltonian. The nominal band gap of the quantum dot, i.e., the energy separation between HOMO and LUMO, is found to be $\Delta_{sp} = 2.26$ eV, which is much larger than that of a bulk phosphorene sheet due to the quantum confinement effect. The system of N_e interacting electrons, as described by

$$\hat{H} = \sum_{m=1}^{N_e} \hat{H}_e(m) + \sum_{m<n}^{N_e} \hat{V}(|\mathbf{r}_m - \mathbf{r}_n|), \quad (3)$$

shall be solved by a configuration interaction (CI) approach. All the 2D artificial materials, including graphene and phosphorene, share one unique advantage over conventional three-dimensional semiconductors, i.e., the strength of electron-electron interactions inside the nanostructures substantially relies on their embedding dielectric environment. Here the intersite (long-range) Coulomb interaction between electrons m and n is screened by the effective dielectric constant κ from the substrate or solution. When $\mathbf{r}_m = \mathbf{r}_n$, the on-site (short-range) Coulomb energy, U_0, is basically an interaction energy between two electrons occupying the same $3p$ orbital. As a first-principles calculation has already shown that this energy for the $2p$ orbital in a carbon atom is 17.0 eV [34] while the radius of a phosphorus atom is about three times larger than a carbon one, we hereby set U_0 to be $17.0/3 \approx 5.5$ eV.

In a two-dimensional system, the electron screening can be substantially different from that in the three-dimensional counterpart. In this sense the Rytova-Keldysh (RK) potential [35,36] is often regarded as a better description of long-range electron-electron interaction when monolayer transition-metal dichalcogenides (TMDs) or graphene is suspended in air or encapsulated between dielectric materials, taking the following form:

$$\hat{V}(r) = k\frac{\pi e^2}{2r_0}\left[H_0\left(\frac{r}{r_0/\kappa}\right) - Y_0\left(\frac{r}{r_0/\kappa}\right)\right], \quad (4)$$

where H_0 and Y_0 are the zero-order Struve and Neumann special functions, $r_0 = 2\pi\chi_{2D}$ is the screening length, and the in-plane polarizability χ_{2D} is set to be 4.1Å [37].

With both the long-range and short-range parts of the interactions setting up, one can define the Coulomb matrix elements as follows:

$$U_{ijkl} = \langle\psi_i(1)\psi_j(2)|\hat{V}(|\mathbf{r}_1 - \mathbf{r}_2|)|\psi_k(1)\psi_l(2)|\rangle. \quad (5)$$

The previously obtained single-particle states are used to construct a series of many-particle configurations (Slater

determinants), such as

$$\Phi_m = \{\phi_{m_1}, \phi_{m_2}, \ldots, \phi_{m_{N_e}}\}, \tag{6}$$

on which the many-particle wave functions are expanded and solved by the CI approach [12]. The QP gap can be obtained thereafter by

$$\Delta_{qp} = \mu(N_e + 1) - \mu(N_e), \tag{7}$$

where the chemical potentials of the system $\mu(N_e)$ and $\mu(N_e + 1)$ are defined by

$$\begin{aligned} \mu(N_e) &= E_g(N_e) - E_g(N_e - 1), \\ \mu(N_e + 1) &= E_g(N_e + 1) - E_g(N_e). \end{aligned} \tag{8}$$

III. RESULTS AND DISCUSSION

By including up to the fourth order ($m = 4$) of excitations among the $N_s = 40$ single-particle states, the total number of configurations reaches beyond 22 million, and the resulting CI matrix is solved with our parallel algorithm to obtain the energy levels of the many-electron system. The quasiparticle shift concerns only the ground-state energies of systems with various numbers of electrons, and in the meantime the energy of the ground state calculated by the CI approach often shows rapid convergence. At $\kappa = 5.0$, for example, Δ_{qs}, calculated by using fewer single-particle states ($N_s = 36$, $m = 4$), gives a value only higher than about 0.05%. By including up to the fifth order of excitations ($m = 5$), the difference between the results is also about 0.05%. Hereby, the calculation by using ($N_s = 40$, $m = 4$) is believed to give well-converged results.

Figure 1 plots the QP shifts Δ_{qs} as a function of the inverse of the effective dielectric constant κ^{-1} by using the RK potential (circular dots) for the hexagonal PQD, as depicted in the inset. For comparison, the result obtained by using the conventional Coulomb interaction potential ($ke^2/\kappa r$) are shown in diamond dots. As the RK potential is known to better describe the electron-electron interactions in two-dimensional systems only when the screening effect is not weak, here we decide to keep the upper limit of κ^{-1} to around 0.2. In this case, our CI method shall be good enough to obtain satisfying results.

At first Δ_{qs} is seen to increase with the weakening screening effect, or decreasing κ in both the RK and conventional Coulomb potentials, as usually expected. However, around $\kappa = 15.0$, the QP shifts are found to reach their maximum values and start to decrease when the screening effect is further suppressed. This is an accelerated decrease, which finally leads to that Δ_{qs} becomes negative at around $\kappa = 6.9$ in the case of conventional Coulomb potential. For the RK potential, the decrease is slower and the QP shift turns out to be negative when $\kappa \leqslant 5.0$. The results obtained by using the two different screening models are seen to be quite similar when κ^{-1} is small and start to deviate from each other until $\kappa \leqslant 10.0$, which is expected because the RK potential would reduce to the conventional Coulomb potential in the presence of a strong screening effect.

As the QP effect arises from the electron-electron interactions, it is usually taken for granted that the QP gap Δ_{qp} shall become larger when the interaction intensity or κ^{-1} increases and the corresponding shift Δ_{qs} shall be always positive.

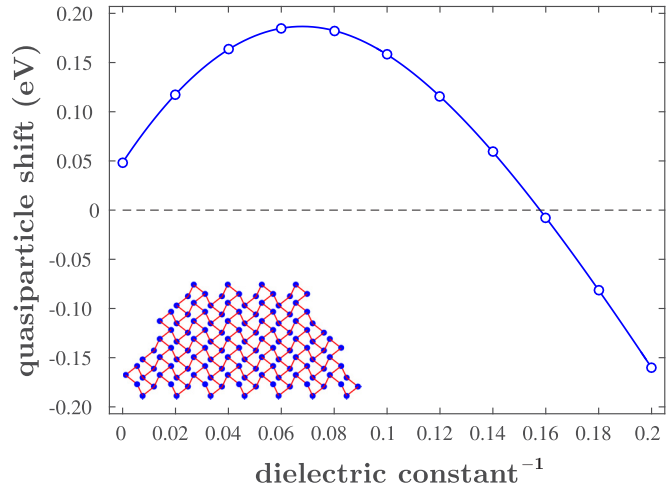

FIG. 2. Quasiparticle shifts calculated as a function of the inverse of the effective dielectric constant for a trapezoidal phosphorene quantum dot as depicted in the inset. The nominal gap of the PQD is 2.1 eV.

However, here we reveal that $\Delta_{qs}(\kappa^{-1})$ no longer remains a monotonically increasing function, and surprisingly, the QP shifts may even become negative when κ is small enough.

To make sure that the anomalous behavior of $\Delta_{qs}(\kappa^{-1})$ is universal for PQDs and not only true for some particular systems, we carry out similar calculations for other PQDs of different geometries, i.e., trapezoid, triangle, and rectangle. Figure 2 plots the QP shift as a function of the inverse of the effective dielectric constant calculated for a trapezoidal PQD as depicted in the inset. The total number of phosphorus atoms is $N = 124$ in this system, which is a little larger than the previous hexagonal one. For simplicity, only the result obtained by using the Coulomb potential is depicted. $\Delta_{qs}(\kappa^{-1})$ is found to exhibit very similar behavior, i.e., at first increasing, quite rapidly reaching its maximum at around $\kappa = 14.7$, afterwards almost linearly decreasing. When $\kappa \leqslant 6.3$, the QP shift is seen to become negative. Both points are seen to be quite close to the previous system.

Figure 3 plots the QP shift as a function of the inverse of the effective dielectric constant calculated by using the Coulomb potential for a triangular PQD as depicted in the inset. There are $N = 5$ rings along the zigzag edge of the dot, and the total number of phosphorus atoms is $N = 80$ in this system. It is a little smaller than the two previous dots. Again, $\Delta_{qs}(\kappa^{-1})$ is found to exhibit very similar behavior, i.e., at first increasing, quite rapidly reaching its maximum at around $\kappa = 9.3$, and afterwards almost linearly decreasing. When $\kappa \leqslant 4.7$, the QP shift is seen to become negative. Both points are seen to be much smaller than the previous systems.

Lastly, we discuss the rectangular PQD. Figure 4 plots the QP shifts calculated as a function of the inverse of the effective dielectric constant for a rectangular PQD as depicted in the inset. The size of the PQD is similar to the first system, and the total number of phosphorus atoms is 98. Here, the results obtained by using both the conventional Coulomb interaction potential and RK potential are shown for comparison. The dependence of the QP shifts on the screening intensity in this rectangular PQD is found to be quite similar to the previous

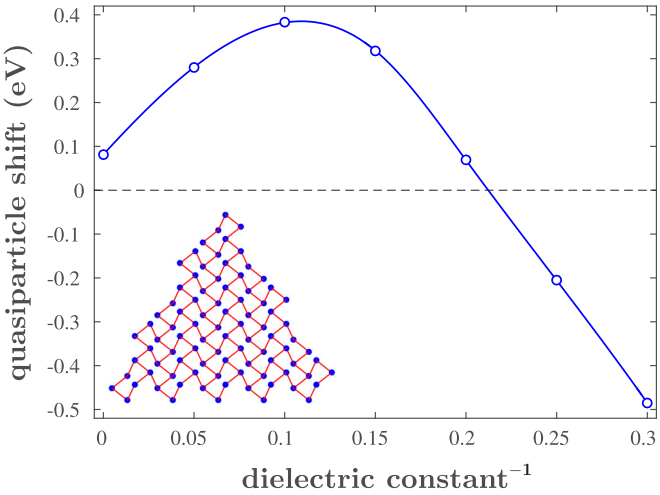

FIG. 3. Quasiparticle shifts calculated as a function of the inverse of the effective dielectric constant for a triangular phosphorene quantum dot as depicted in the inset. The nominal gap of the PQD is 2.44 eV.

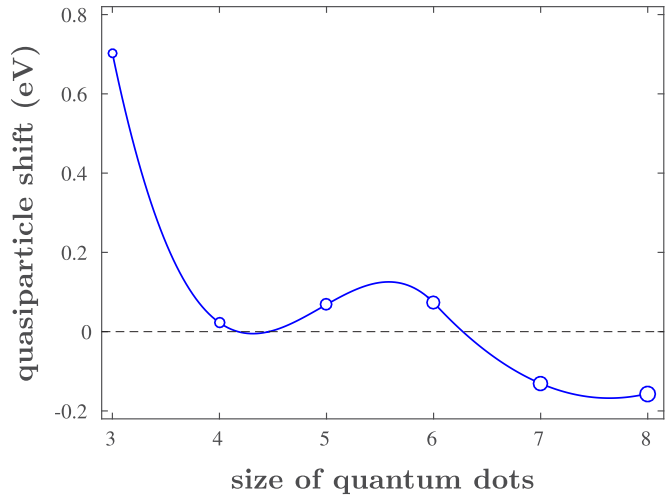

FIG. 5. Quasiparticle shifts calculated as a function of the size of triangular phosphorene quantum dot for the effective dielectric constant set as 5.0. The total number of atoms starts from 30 in the smallest PQD to 200 in the largest one. Correspondingly, the nominal gap of PQDs decreases from 3.28 to 1.99 eV. The lines depicted are only to guide the eye.

systems. The result by using the conventional Coulomb potential shows that Δ_{qs} becomes negative at around $\kappa = 6.9$ while that obtained from the RK potential turns out to be negative until $\kappa \leqslant 6.0$. Compared with the first hexagonal system, the results obtained by using the two different interaction models are seen to deviate from each other at a smaller value of κ (8.0).

The anomalous behavior of $\Delta_{qs}(\kappa^{-1})$ has now been seen in the PQDs with all four geometries. Except for the triangular dot, the values of κ at which the quasiparticle shift becomes negative are quite close to each other for all the PQDs. After seeing the geometrical effect, it is worthwhile to study the dimensional dependence of the quasiparticle shift. Figure 5 plots the quasiparticle shifts calculated by using the Coulomb potential as a function of the size of triangular PQDs (number of rings along the zigzag edge). At the effective dielectric constant set to be $\kappa = 5.0$, Δ_{qs} is seen to change from 0.70 eV in the smallest PQD ($N_e = 30$) to -0.156 eV in the largest dot ($N_e = 200$). Although the dependence is not totally monotonic and is sometimes oscillating, we find that the quasiparticle shift roughly decreases with the size of PQDs.

Hereby we see that the QP shift exhibits complicated dependence on the intensity of long-range electron-electron interactions. To find how Δ_{qs} relies on the short-range interactions or the on-site Coulomb energy U_0, we fix κ^{-1} at 0.12 and calculate the dependence of Δ_{qs} on U_0. Figure 6 plots the relative change of the QP shift calculated as a function of the on-site Coulomb energy for the same rectangular PQD. Unlike

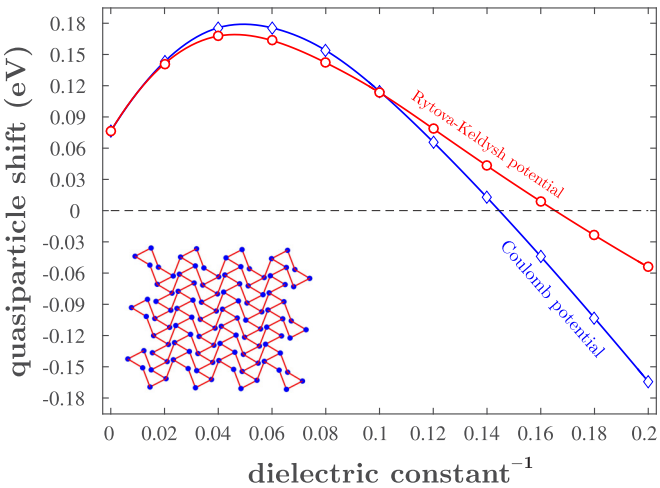

FIG. 4. Quasiparticle shifts calculated as a function of the inverse of the effective dielectric constant for a rectangular phosphorene quantum dot as depicted in the inset. The nominal gap of the PQD is 2.48 eV.

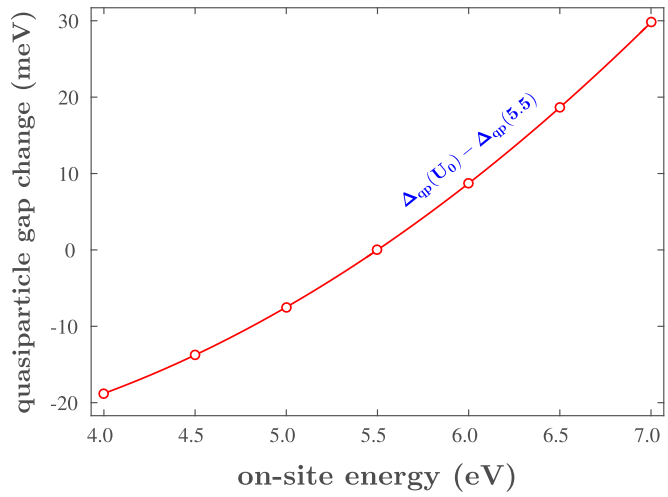

FIG. 6. The relative change of the quasiparticle shift calculated as a function of the on-site Coulomb energy when $\kappa^{-1} = 0.12$ for the rectangular phosphorene quantum dot, as depicted in Fig. 4. The nominal gap of the PQD is 2.48 eV.

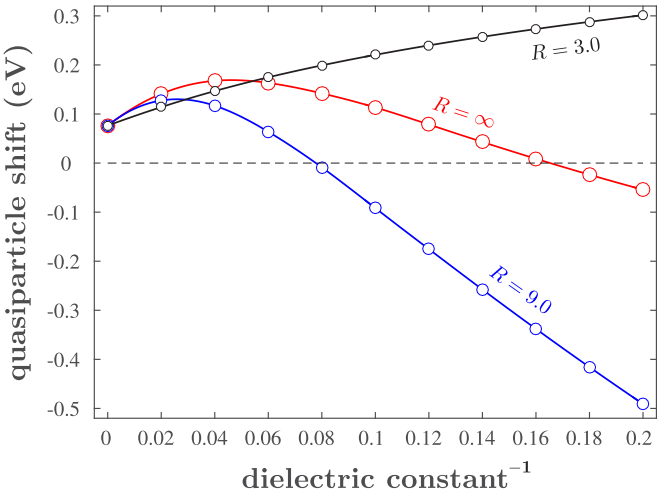

FIG. 7. At various values of the cut-off distance in the RK interaction potential, quasiparticle shifts calculated as a function of the inverse of the effective dielectric constant for the rectangular phosphorene quantum dot with a nominal gap of 2.48 eV.

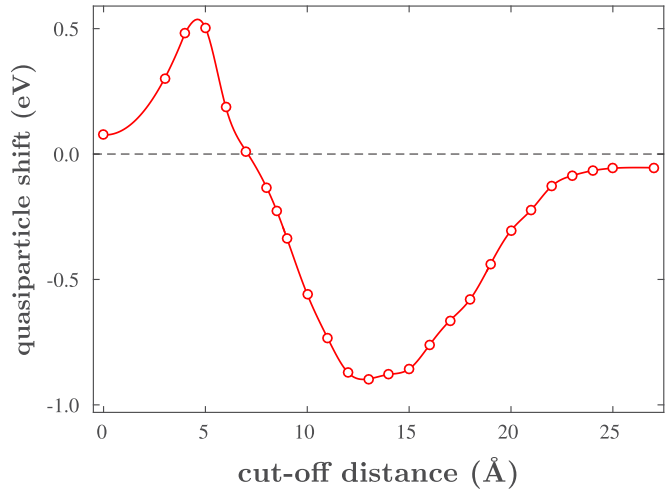

FIG. 8. Quasiparticle shifts calculated as a function of the cutoff distance in the RK interaction potential at $\kappa = 5.0$ for the rectangular phosphorene quantum dot with a nominal gap of 2.48 eV. The lines depicted are only to guide the eye.

$\Delta_{qs}(\kappa^{-1})$, as previously revealed, the QP shift is now shown to increase monotonically with the on-site interaction energy, which has been expected in the first place.

Now it is clear that the long-range interactions shall be responsible for the anomalous dependence of Δ_{qs} on the screening intensity and even the negative QP shifts. To explore further, we introduce a cut-off distance R to the RK interaction potential $V(r)$, i.e., $V(r) = 0$ when $r \geqslant R$. At various values of R we calculate the dependence $\Delta_{qs}(\kappa^{-1})$ to see which part of the potential leads to the negative Δ_{qs}. Figure 7 plots the results for three different values of the cut-off distance, namely, $R = 3.0$ Å, $R = 9.0$ Å, and $R = \infty$. The last one corresponds to no cut-off in the interaction potential, which is already shown in Fig. 4 and depicted here only for comparison.

In BP nanostructures, the nearest and next nearest distances among the P atoms are given by 2.22 Å and 2.24 Å, respectively. Hence the case of $R = 3.0$ Å represents the typical short-range interaction, and the corresponding $\Delta_{qs}(\kappa^{-1})$ is shown to be a monotonically increasing function. It is within the expectation, judging from the result on the on-site energy as shown in Fig. 6. In this rectangular PQD model, the maximum distance among the atoms is about 27.0 Å. The case of $R = 9.0$ Å is therefore related to the typical middle-range interaction. Compared with the no cut-off case ($R = \infty$), the QP shift is seen to reach its climax much earlier and then decrease more rapidly. It is quite surprising, as one expected a simple dependence of the QP shift on the cut-off distance. Although it is hard to separate the contributions of different parts of the interaction potential from each other, in regard to the QP shift, one may draw a conclusion that the origin of this anomalous QP shift shall be related with the long-range electron-electron interactions in the distinctive lattice structure of PQDs.

To obtain a more quantitative understanding of how the long-range interactions affect the QP shift, we calculate $\Delta_{qs}(R)$ at a fixed κ. Figure 8 plots the QP shifts calculated as a function of the cut-off distance in the RK interaction potential at $\kappa = 5.0$ for the same PQD model. As the distances among the atoms in the BP lattice take discrete values, the curvature detail of the dependence is irrelevant, and the lines depicted are only to guide the eye. It is noted that the low-distance part of the results has no physical meaning and is shown here only for comparing the effects of small and large cut-off distances.

As can be seen from the result, Δ_{qs} exhibits quite a complicate dependence on the screening length or the cut-off distance in the interaction potential. At first, one finds that the QP shift would definitely be enhanced if the potential consists of only the short-range part. However, beyond about $R = 5.0$ Å, the middle-range part of the interaction potential is seen to suppress Δ_{qs} quite rapidly until around $R = 13.0$ Å. Beyond this point, the potential tail actually becomes very weak. However, it is shown that the long-range part of the interaction potential enhances the QP effect in almost the same manner as the short-range part does. In spite of that, the QP shift remains negative if all the parts of the interaction potential are taken into account.

IV. CONCLUSION

In summary, we have investigated quasiparticle effect in phosphorene quantum dots by using a configuration interaction approach beyond the conventional double-excitation scheme. Contrary to the common belief that enhanced electron correlations would open up a quasiparticle gap, for the hexagonal PQD with a nominal gap of 2.26 eV, we have shown that the quasiparticle shift decreases from 0.22 to −0.30 eV when the effective dielectric constant is reduced from 20.0 to 5.0. For other trapezoidal, triangular, and rectangular PQDs, we have found that the QP shift exhibits a similar amount of decrement after the same change in the dielectric environment. We reiterate that a similar phenomenon has not been found in other 2D nanostructures such as graphene quantum dots. After examining the dependence of the QP shift in the interaction potential with different cut-off distances, we

believe that the origin of this anomalous quasiparticle shift is related with the long-range electron-electron interactions in the distinctive lattice structure of PQDs.

ACKNOWLEDGMENT

This work is supported by National Natural Science Foundation of China (Project No. 12074078).

[1] P. Wölfle, Rep. Prog. Phys. **81**, 032501 (2018).
[2] A. L. Fetter and J. D. Walecka, *Quantum Theory of Many-Particle Systems* (Dover, New York, 2003).
[3] S. Sharifzadeh, A. Biller, L. Kronik, and J. B. Neaton, Phys. Rev. B **85**, 125307 (2012).
[4] L. Yang, C.-H. Park, Y.-W. Son, M. L. Cohen, and S. G. Louie, Phys. Rev. Lett. **99**, 186801 (2007).
[5] R. S. Knox, *Solid State Physics: Supplement* (Academic Press, New York, 1963), Vol. 5.
[6] C. Sun, F. Figge, J. A. McGuire, Q. Li, and L.-S. Li, Phys. Rev. Lett. **113**, 107401 (2014).
[7] P. Vishnoi, M. Mazumder, M. Barua, S. K. Pati, and C. N. R. Rao, Chem. Phys. Lett. **699**, 223 (2018).
[8] J.-H. Choi, P. Cui, H. Lan, and Z. Zhang, Phys. Rev. Lett. **115**, 066403 (2015).
[9] Z. Jiang, Z. Liu, Y. Li, and W. Duan, Phys. Rev. Lett. **118**, 266401 (2017).
[10] W. Sheng and H. Wang, Phys. Chem. Chem. Phys. **18**, 28365 (2016).
[11] W.-T. Hsu, J. Quan, C.-Y. Wang, L.-S. Lu, M. Campbell, W.-H. Chang, L.-J. Li, X. Li, and C.-K. Shih, 2D Mater. **6**, 025028 (2019).
[12] W. Sheng, M. Sun, A. Zhou, and S. J. Xu, Appl. Phys. Lett. **103**, 143109 (2013).
[13] L. K. Li, Y. J. Yu, G. J. Ye, Q. Q. Ge, X. D. Ou, H. Wu, D. L. Feng, X. H. Chen, and Y. B. Zhang, Nat. Nanotechnol. **9**, 372 (2014).
[14] F. Xia, H. Wang, and Y. Jia, Nat. Commun. **5**, 4458 (2014).
[15] M. Buscema, D. J. Groenendijk, S. I. Blanter, G. A. Steele, H. S. J. van der Zant, and A. Castellanos-Gomez, Nano Lett. **14**, 3347 (2014).
[16] Y. Xu, Z. Wang, Z. Guo, H. Huang, Q. Xiao, H. Zhang, and X.-F. Yu, Adv. Opt. Mater. **4**, 1222 (2016).
[17] X. Zhang, H. Xie, Z. Liu, C. Tan, Z. Luo, H. Li, J. Lin, L. Sun, W. Chen, Z. Xu, L. Xie, W. Huang, and H. Zhang, Angew. Chem. Int. Ed. **54**, 3653 (2015).
[18] Z. Sofer, D. Bouŝa, J. Lux, V. Mazanek, and M. Pumera, Chem. Commun. **52**, 1563 (2016).
[19] S. Ge, L. Zhang, P. Wang, and Y. Fang, Sci. Rep. **6**, 27307 (2016).
[20] W. Hu, L. Lin, C. Yang, J. Dai, and J. Yang, Nano Lett. **16**, 1675 (2016).
[21] B. Rajbanshi, M. Kar, P. Sarkar, and P. Sarkar, Chem. Phys. Lett. **685**, 16 (2017).
[22] J. Du, M. Zhang, Z. Guo, J. Chen, X. Zhu, G. Hu, P. Peng, Z. Zheng, and H. Zhang, Sci. Rep. **7**, 42357 (2017).
[23] R. Zhang, X. Y. Zhou, D. Zhang, W. K. Lou, F. Zhai, and K. Chang, 2D Mater. **2**, 045012 (2015).
[24] Z. T. Jiang, S. Li, Z. T. Lv, and X. D. Zhang, AIP Adv. **7**, 045122 (2017).
[25] L. L. Li, D. Moldovan, W. Xu, and F. M. Peeters, Phys. Rev. B **96**, 155425 (2017).
[26] J.-H. Lin, H. Zhang, and X.-L. Cheng, Front. Phys. **10**, 107301 (2015).
[27] X. Niu, Y. Li, H. Shu, and J. Wang, J. Phys. Chem. Lett. **7**, 370 (2016).
[28] V. A. Saroka, I. Lukyanchuk, M. E. Portnoi, and H. Abdelsalam, Phys. Rev. B **96**, 085436 (2017).
[29] Y. Zhang and W. Sheng, Phys. Rev. B **97**, 205424 (2018).
[30] A. N. Rudenko, S. Yuan, and M. I. Katsnelson, Phys. Rev. B **92**, 085419 (2015); **93**, 199906 (2016).
[31] J. Zhong and W. Sheng (unpublished).
[32] C. J. Pàez, K. DeLello, D. Le, A. L. C. Pereira, and E. R. Mucciolo, Phys. Rev. B **94**, 165419 (2016).
[33] G. Zhang, A. Chaves, S. Huang, F. Wang, Q. Xing, T. Low, and H. Yan, Sci. Adv. **4**, eaap9977 (2018).
[34] T. O. Wehling, E. Şaşıoğlu, C. Friedrich, A. I. Lichtenstein, M. I. Katsnelson, and S. Blügel, Phys. Rev. Lett. **106**, 236805 (2011).
[35] N. S. Rytova, Proc. MSU Phys. Astron. **3**, 30 (1967).
[36] L. V. Keldysh, JETP Lett. **29**, 658 (1979).
[37] M. N. Brunetti, O. L. Berman, and R. Y. Kezerashvili, Phys. Rev. B **100**, 155433 (2019).